European Commission

JRC TECHNICAL REPORTS

Modelling Toolbox 2: The Black Sea ecosystem model

Svetla Miladinova
Adolf Stips
Elisa Garcia-Gorriz
Diego Macias Moy

2016

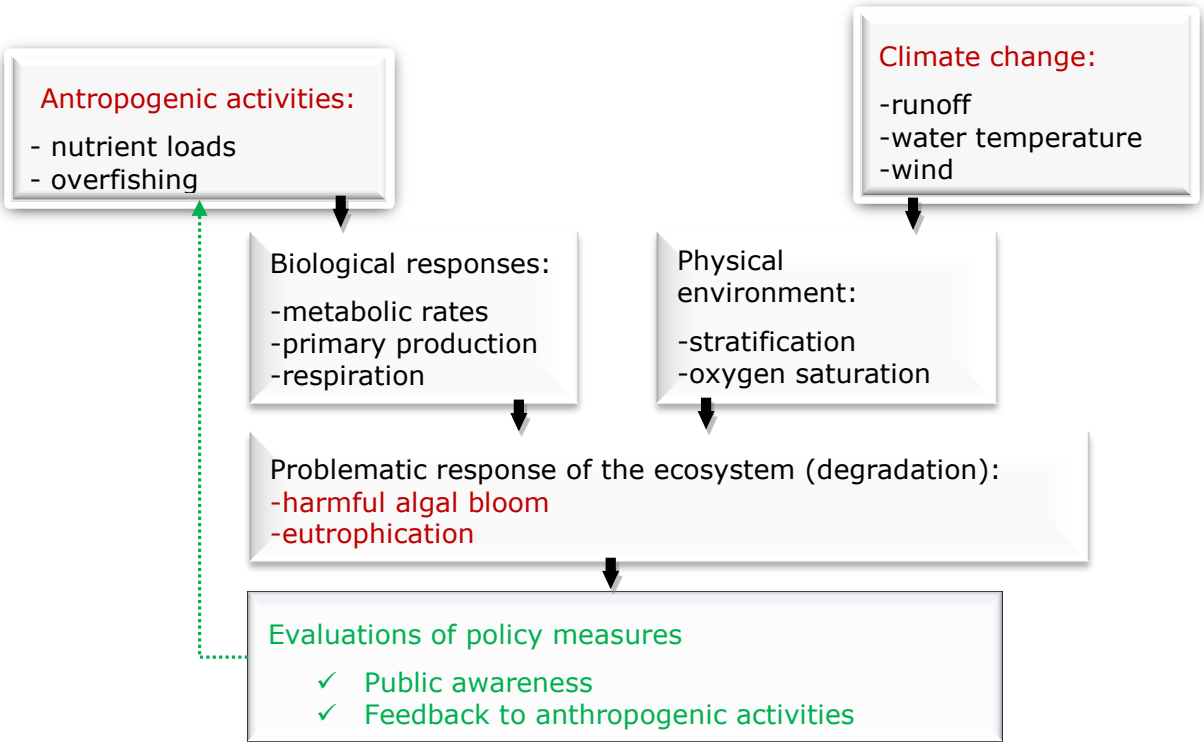

EUR 28372 EN

Joint Research Centre

Modelling Toolbox 2: The Black Sea ecosystem model

Contact information
Name: S. Miladinova
Address: Joint Research Centre, Via E. Fermi, 2749 – TP27, 21021 Ispra (VA), Italy
E-mail: svetla.miladinova@jrc.ec.europa.eu
Tel.: +39 0332 78 5347

JRC Science Hub
https://ec.europa.eu/jrc

JRC104987

EUR 28372 EN

PDF	ISBN 978-92-79-64669-0	ISSN 1831-9424	doi:10.2788/677808
Print	ISBN 978-92-79-64668-3	ISSN 1018-5593	doi:10.2788/069961

Luxembourg: Publications Office of the European Union, 2016

How to cite: Svetla Miladinova, Adolf Stips, Elisa Garcia-Gorriz, Diego Macias Moy; *Modelling Toolbox 2: The Black Sea ecosystem model*; EUR 28372 EN; doi:10.2788/677808

Table of contents

Acknowledgements

We acknowledge Prof. Temel Oguz for making available the general structure of the BSEM model. The first author is supported by Marie Curie research funding in the framework of the EU-MC 33764 SIMSEA project. We thank to "The Global Runoff Data Centre, 56068 Koblenz, Germany" for the Danube daily discharge rates. Special thanks go to the GETM, GOTM and FABM developers for providing and maintaining the model.

Abstract

The Marine Strategy Framework Directive (MSFD) obligates all EU Member States to take the necessary measures to maintain or progressively achieve Good Environmental Status (GES) in the marine environment by the year 2020. In order to assist Member States (MSs) in the implementation of the MSFD, a MSFD Competence Centre (MCC, http://mcc.jrc.ec.europa.eu/) has been established at the Joint Research Centre, Directorate D – Sustainable Resources (Water and Marine Resources Unit). In the framework of the Administrative Arrangement No ENV C.2/2015/070201/705766 between DG Environment and DG JRC, Directorate D – Sustainable Resources, Water and Marine Resources, the development of a modelling toolbox has been initiated. This toolbox facilitates the online coupling of a hydrodynamic model with a lower trophic level model of the Black Sea ecosystem. It can be used for multi-annual simulations of past, present and future conditions in the Black Sea. The General Estuarine Transport Model (GETM) has been selected as reliable hydrodynamic model for the Black Sea's simulations. The model is forced with atmospheric data from the European Regional Downscaling Experiment (EURO-CORDEX), river runoff from Global Runoff Data Centre (GRDC) and is initialised with temperature and salinity 3D fields coming from the project MEDAR/MEDATLAS II. A new Black Sea Ecosystem Model (BSEM) is linked via the Framework for Aquatic Biogeochemical Models (FABM,) with the hydrodynamic model. The coupled physical-ecosystem modelling system has been calibrated and validated for the Black Sea conditions. The numerical experiments indicate that the biogeochemical components of the model rather successfully reproduce the main features and state variable evolution in the Black Sea ecosystem: the growth in phytoplankton biomass and changes in seasonal cycles of the main ecosystem components. It is however shown, that the physical processes are of fundamental importance for a reliable reproduction of seasonal and inter-annual changes in the ecosystem.

1. Introduction

A vision for clean, healthy, safe, productive and biologically diverse oceans and seas is the basis for managing sustainable human use and exploitation of the goods and services provided by the seas. Numerical modelling supports the development of methods to describe the state of the ecosystem and mechanisms to minimize the impacts of human activities to avoid undesirable disturbances. The marine models developed within the Water Resources unit could be used to highlight regions at high risk of physical and biochemical change, such as oxygen depletion events and eutrophication. Development of a marine knowledge base that focuses on physically and biologically sensitive areas is necessary to support marine spatial planning measures that integrate ecosystem and biodiversity conservation with economic activities. Marine modelling at JRC provides a tool to examine the marine ecosystem and results from the various setups can inform and support a variety of EU policies including the Marine Strategy Framework Directive (MSFD). The Modelling Framework (MF) for EU regional seas has being developed by DG JRC (Garcia-Gorriz et al., 2016; Stips et al., 2015). This MF could be used to assess the current status of several descriptors included in the definition of Good Environmental Status (GES) in the context of the MSFD. Since in Europe the implementation process of the MSFD in the Black Sea region is the least developed we focus for this project on the marine ecosystem of the Black Sea. Further developments, including a biogeochemical coupled model, would be used in the future to evaluate policy options in scenario mode in order to obtain forecast simulations of alternative states of the basin in the future.

The Black Sea's ecosystem has experienced substantial changes since the 1960s, such as nutrient enrichment and large population growth of gelatinous and opportunistic species. Most likely excessive anthropogenic nutrient loading and overfishing contributed to this ecological degradation. Evidently, those changes are deeply influenced by climate change (Oguz et al., 2006). Climate change modulates primary production in marine systems through three main mechanisms - direct physiological responses to changes in water temperature and salinity (e.g. temperature controls on phytoplankton growth rates); water column stability and processes of vertical transport (e.g. nutrient re-supply from below the euphotic zone, oxygen penetration depth, the exposure of phytoplankton to light, etc.); and circulation processes which distribute nutrient rich water masses such as arising from river plumes (Holt et al., 2014). Climate affects the Black Sea via atmospheric transfer and riverine inflow. The later has been a significant factor for the overall water balance and basin-scale circulation (Oguz et al., 1995). The physical environment of the Black Sea has a major influence across the food web at different time scales (Daskalov, 2003) and has been shown to be influenced by the Atlantic climate through cross-Europe atmospheric teleconnections (Polonsky et al., 1997; Oguz et al., 2006).

Different aspects of the structural changes observed in the Black Sea ecosystem have been studied quantitatively by modelling studies (e.g. Oguz et al., 2000 and 2001; Oguz and Merico, 2006; Lancelot et al., 2002; Gregoire et al., 2004; Gregoire et al., 2008; Staneva et al., 2010; He et al., 2012). A common feature of the existing numerical models for the Black Sea dynamics is the relaxation to observational data (mainly to salinity fields). Even more recent model versions still use surface salinity relaxation mainly because of the difficulty in reproducing correctly the surface salinity and especially the high vertical salinity gradients. Thus the Black Sea's surface salinity evolution is not studied adequately because all historical simulations depend on availability and accuracy of scarce measurements. Even more restrictive is, that the observational evidence can be only used for relaxation in hindcast simulations, however for potential future climate change scenarios no measured data are available. The realistic simulation of temperature and salinity fields is also important for the nutrients budget in the Black Sea, which is in turn important for the phytoplankton bloom and hence the changes in regional ecological characteristics (e.g., Oguz et al., 2004 and 2006).

The Black Sea numerical simulations are typically focussed on a specific site in the Black Sea, particular species or on a certain time period (Lancelot et al., 2002; Gregoire et al., 2004; Gregoire et al., 2008). Moreover, they do not address the eutrophication problem in general and the complexity of main processes governing phytoplankton blooms and its temporal and spatial variability.

The aim of the modelling team is to develop a toolbox that is linking a new advanced ecosystem model for the complex Black Sea ecosystem (BSEM) and the validated JRC hydrodynamic model (GETM). This coupled model needs to be capable to run future scenario simulations considering different policy options and climate change scenarios. To achieve this ambitious goal, we first have to choose the forcing data sets, define model parameters for key processes, and test and validate the model.

2. Materials and Methods

2.1 Study area and hydrography

The Bosphorus Strait connects the Black Sea with the Mediterranean Sea via the Marmara Sea and the Kerch Strait is the connection with the Azov Sea (Fig.1). The shelf edge slope is steep and the shelf is basically narrow except for the north-western shelf region. In this region several big rivers discharge, namely, the Danube, Dniepr and Dniestr. In addition to these rivers, the Rioni, Sakarya, Kizil Irmak, Coruhsuyu, Yesilirmak and many other small ones discharge into the Black Sea. Buoyancy input due to river runoff is an essential reason for the basin wide cyclonic circulation the so called Rim Current with well exhibited western and eastern gyres (Oguz, 1995). The general circulation of the Black Sea is driven by this large freshwater input on the north-western shelf as well as wind stress and is determined by the steep topography around its periphery that consists of narrow shelves and a maximum depth of around 2200 m (Oguz et al., 2004). The eddy dominated circulation exhibits different types of structural organizations within the interior cyclonic cell, the Rim Current flowing and meandering along the sharply varying topography. The interior circulation comprises several sub-basin scale gyres, each of them involving a series of cyclonic eddies that interact among each other. The presence of a series of recurrent, near-shore, anti-cyclonic eddies between the Rim Current and the coast, along with a number of cyclonic gyres in the basin's central area, have been confirmed by satellite data, hydrographic observations and numerical simulations (see the review in Oguz et al., 2004). Defined by temperatures less than 8^{o}C in the sub-surface Black Sea's waters, the Cold Intermediate Layer (CIL) contains the lowest temperatures and most of the Black Sea's pycnocline (Oguz et al., 1992). The Black Sea is characterised by a positive fresh water balance that results in a net outflow into the Mediterranean. With a drainage basin five times more extensive than the sea area (Ludwig et al., 2010) it works as a virtually isolated ecosystem. Two distinct regions can be recognized: the wide and shallow Northwest Shelf (<200 m) and the interior deep sea, which is bounded by the 200 m isobath (Fig. 1). The latter is mostly isolated from the riverine inflow, which is known to be a key driver on the shelf. Note that all basin mean results presented herein are averages over the basin interior with depth > 200 m. However the mesoscale eddies evolving along the periphery of the basin as a part of the Rim current dynamic structure effectively link coastal biogeochemical processes to those in the deep sea and thus provide a mechanism for two-way transport between nearshore and offshore regions (Zatsepin et al., 2003). These regions have been seen to show physical and biological differences (McQuatters-Gollop et al., 2008). Productivity of the shelf system appears to be primarily phosphorus limited whereas the open sea system would appear to be nitrogen limited and much more dependent on mixing processes for nutrient supply (Garnier et al., 2002).

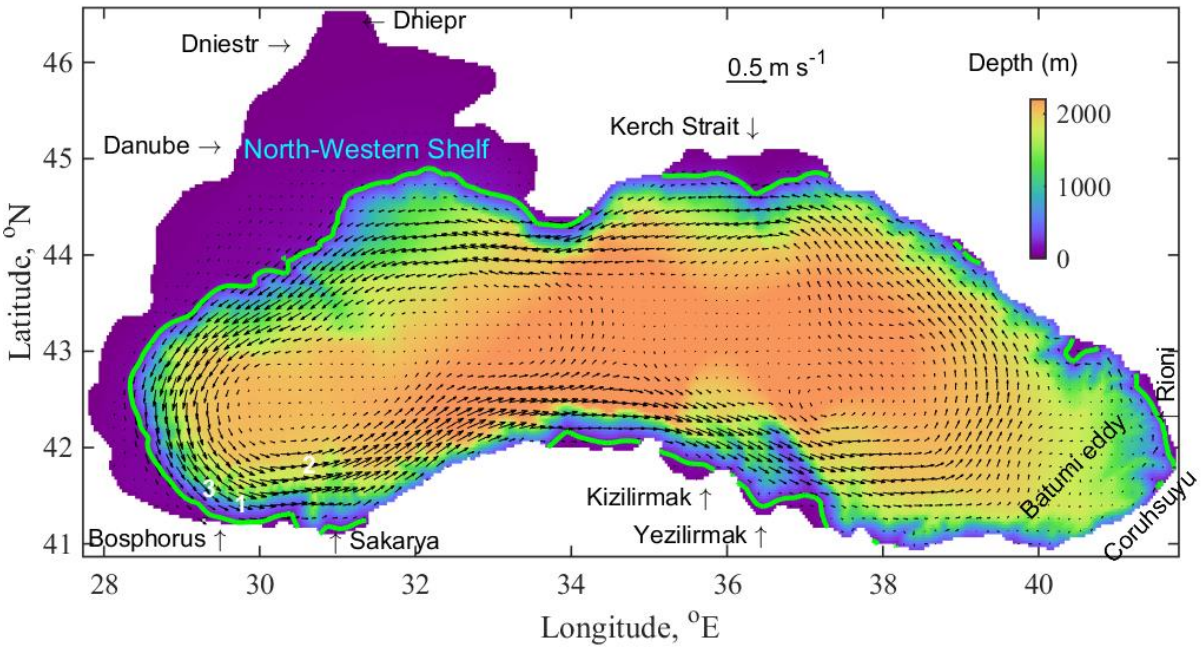

Figure 1. Bathymetry and location map of the Black Sea. The boundary of the shelf and deep sea interior, separated by the 200 m isobath is shown in green. Also shown are climatological mean velocity vectors at 50 m depth in November. The positions of the 2003 R/V Knorr research cruise observations (http://www.ocean.washington.edu/cruises/) used in the study (Fig. 4) are presented with numbers: 1 – Data1, 2 – Data2 and 3 – Data3.

2.2 Model structure

The model involves simultaneous solutions of a set of three-dimensional equations for the physical and ecosystem modules. Our 3D hydrodynamic model comprises of 3D GETM (http://www.getm.eu/) and General Ocean Turbulence Model (GOTM) initialised on high resolution (2 min by 2 min) horizontal grid and with 70 vertical levels. The resultant flow fields from the hydrodynamic model are then used to calculate the evolution of the low trophic level components of the food chain in the Black Sea ecosystem. Black Sea's ecosystem model is linked with the GETM/GOTM hydrodynamic models via the Framework for Aquatic Biogeochemical Models (FABM, Bruggeman and Bolding 2014). FABM is an interface between biogeochemical models and physical models developed to run with GETM/GOTM among many other hydrodynamic models for several computing platforms. To describe the low trophic level pelagic ecosystem model of the Black Sea, a nitrate-based biogeochemical model has been implemented following the existing literature (e.g., Oguz et al., 2000, 2001, 2006, 2008, 2014). This model provides an optimally complex system of food web interactions and biogeochemical cycles comprising oxic-, suboxic- and anoxic waters of the Black Sea. It represents the classical omnivorous food-web with 7 state variables. These include two phytoplankton size groups (small and large), four zooplankton groups including micro- and mesozooplankton, non-edible dinoflagellate species as *Noctiluca,* and the gelatinous zooplankton species *Mnemiopsis.* Nitrogen is represented by two inorganic nutrients (nitrate and ammonium) and included in the particulate organic material (detritus). Additional state variables are dissolved oxygen and hydrogen sulphide. This system offers an optimal complexity with medium complex trophic interactions as shown in Figure 2. The full set of equations describing this ecosystem is given in the Appendix A (and also in Oguz et al., 2014). Hereinafter this model will be referred to as BSEM. BSEM

has been implemented into the FABM and is available for the scientific community through the FABM repository.

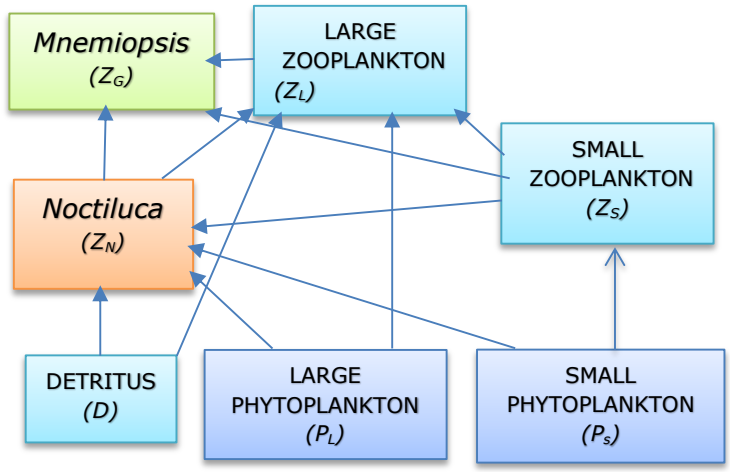

Figure 2. Schematic representation of the BSEM structure that includes the basic omnivorous food web and its interactions with the gelatinous carnivore predator *Mnemiopsis* and *Noctiluca shunt*.

2.3 Model forcing and setup

The quality of the forcing data affecting our simulations has been analysed in *Miladinova-Marinova et al.* [2016b] and *Miladinova et al.* [2016a] and the most appropriate forcing data capable to assess the potential changes in the Black Sea dynamics has been selected.

The meteorological forcing from the European Centre for Medium Range Weather Forecast (ECMWF) available from http://www.ecmwf.int, has been applied, namely, ERA-40 project (1958-1978) and ERA-Interim project (1979-2015). Figure 3 illustrates annual mean values of evaporation/precipitation from 1980 to 2010 extracted from ERA-Interim data set. Evaporation does not vary considerably through the years and datasets, having an absolute average value 2.42 mm day^{-1}. Contrary, precipitation varies considerably – from 1.2 to 1.8 mm day^{-1}

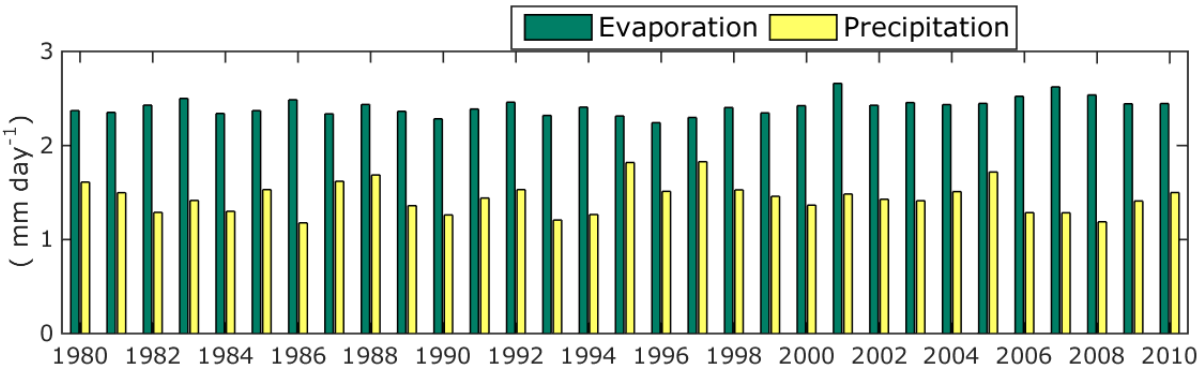

Figure 3. Annual mean values of evaporation and precipitation over the Black Sea calculated using ERA-Interim data.

The hydrodynamic model is initialised by means of temperature and salinity 3D fields coming from the project MEDAR/MEDATLAS II (http://www.ifremer.fr/medar). An accurate method for evaluation of water optical characteristics by means of an optical depth estimated from the satellite data has been involved. Finally, the performance of the model in simulating the Black Sea physical properties at seasonal and inter-annual scales has been assessed (Miladinova-Marinova et al., 2016b). Upper and deep water circulation, thermohaline structure, temporal and space variability of the Rim current and CIL are reasonably simulated by the model.

Freshwater input has been evaluated using the values from the Global Runoff Data Centre (GRDC, http://www.bafg.de/GRDC) runoff. Being an estuarine basin, the Black sea is very sensitive to variations in the fresh water balance. The resulting buoyancy induced movements are essential for establishing the basin circulation, and therefore we have to define adequately the water and salt fluxes at the Bosphorus Strait (Miladinova-Marinova et al., 2016b). Rivers nutrients loads data are issued from the SESAME and PERSEUS projects (Ludwig et al., 2009).

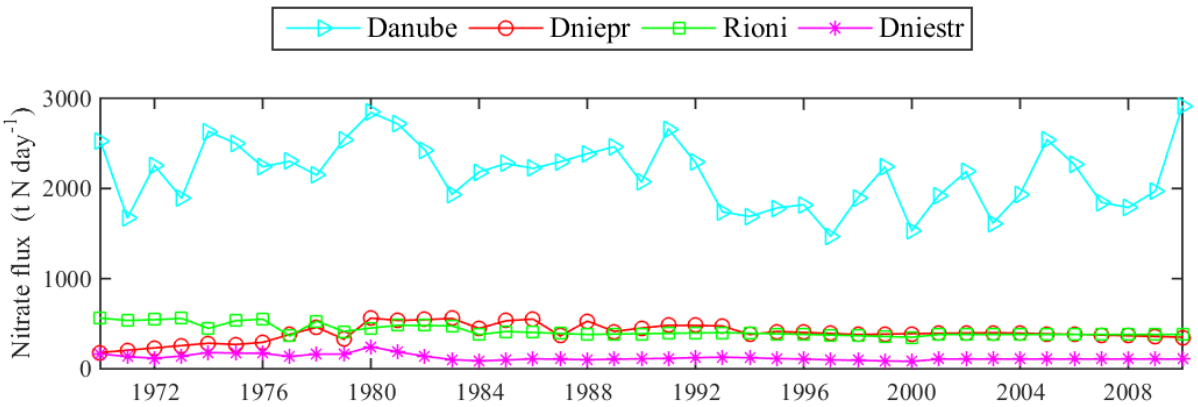

Figure 4. Annual mean nitrate fluxes (t N day^{-1}) of the bigger Black Sea rivers.

In Fig. 4 is given the annual mean daily nitrate flow rate from the four biggest Black Sea rivers. As the flow rate data is missing since 1995 for the most of the big rivers except the Danube, climatological mean values are used instead real data. No nutrient deposition from the atmosphere is considered herein.

The initial conditions of the BSEM variables (Fig.5) are chosen to be similar to Knorr 2001/2003 experimental data (Cannaby et al, 2015; Tugrul et al., 2014; Stanev et al., 2014). They reproduce mainly the observed characteristics near north-western and south-western shelf of the Black Sea ecosystem. Nitrate concentration is set to 0.33 mmol N m^{-3} within the upper 10 m, then it increases to 3.7 mmol N m^{-3} between 15 m and 35 m depths and decreases to zero at 100 m. Ammonium is set to 0.03 mmol N m^{-3} within the upper 90 m, then it increases linearly to 70 mmol N m^{-3} between 90 m and 450 m depths and remains constant till the sea bottom. Hydrogen sulphide is zero in the upper 90 m, then it increases linearly to 860 mmol HS m^{-3} at the sea bottom. Dissolved oxygen decreases linearly from 340 mmol O_2 m^{-3} to 0 in the upper 70 m and is set to zero further below. All the other BSEM state variables are set to small and vertically uniform values over the entire water column because their equilibrium structures do not depend on the initial conditions and are emergent properties of the model dynamics (see Appendix B).

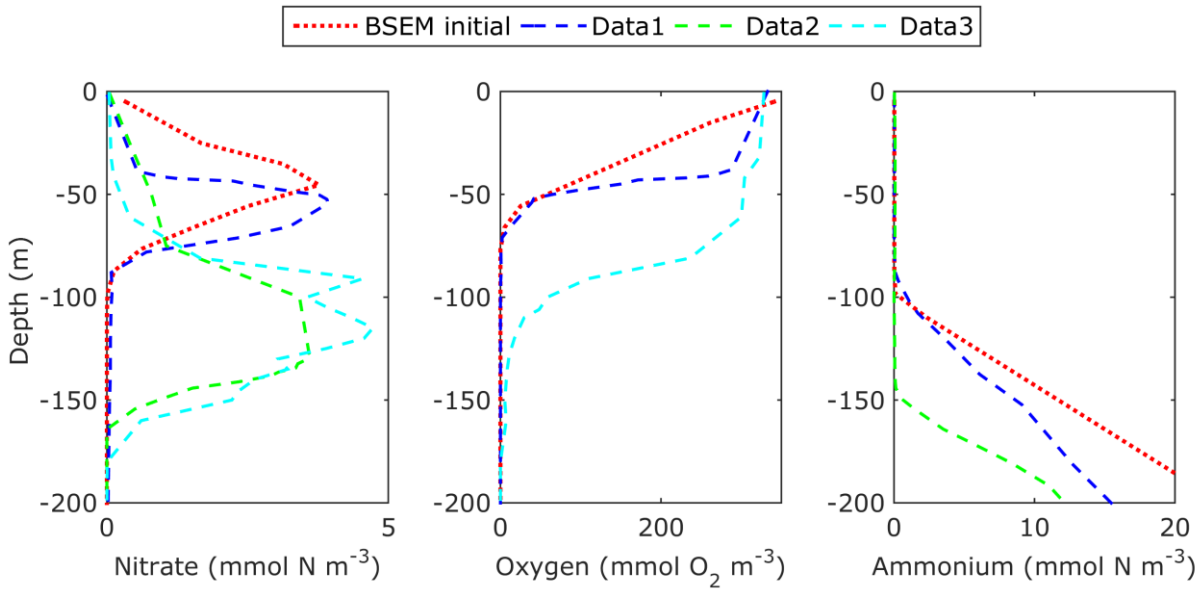

Figure 5. Initial vertical profiles of nitrate (mmol N m^{-3}), oxygen (mmol O_2 m^{-3}) and ammonium (mmol N m^{-3}) from the surface to 200 m depth. Profiles of the 2003 R/V Knorr research cruise observations (see Fig. 1 for the profile locations).

3. Results and verification

An extensive model parameterisation and sensitivity analysis have been done (Miladinova-Marinova et al., 2016b) and the model key parameters have been determined. The final version of the BSEM parameterisation is given in Appendix B.

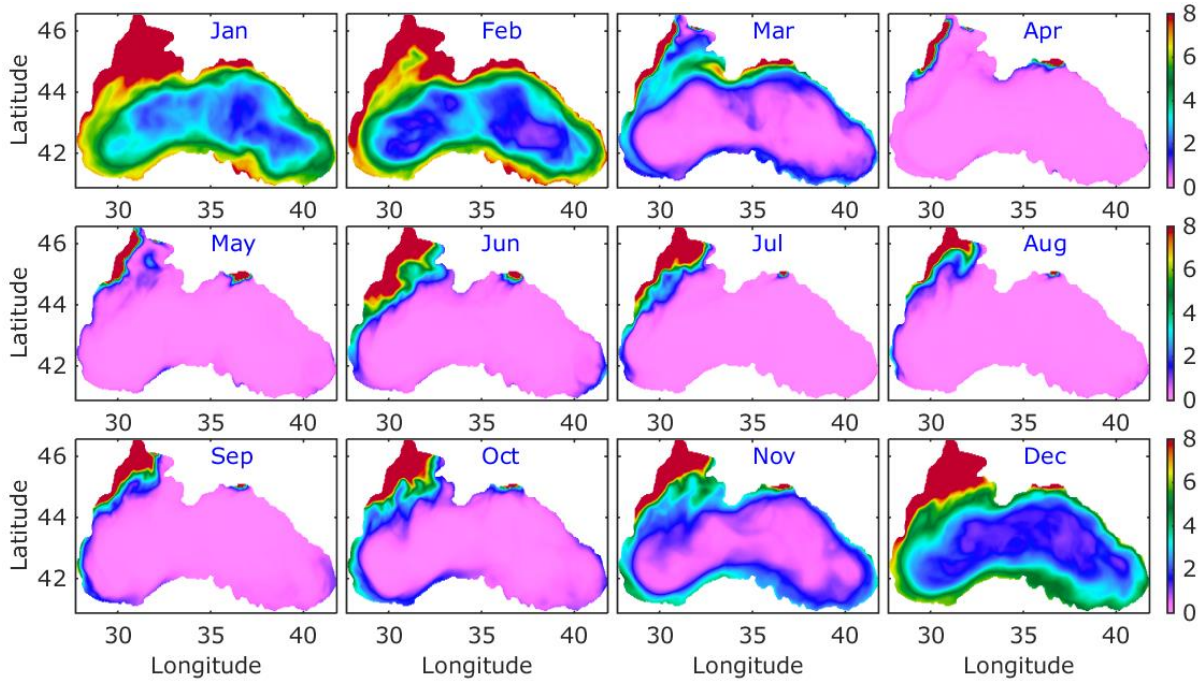

Figure 6. Climatological monthly distribution of nitrate (mmol N m^{-3}) from 2001 to 2010 (simulation with a river nutrient load).

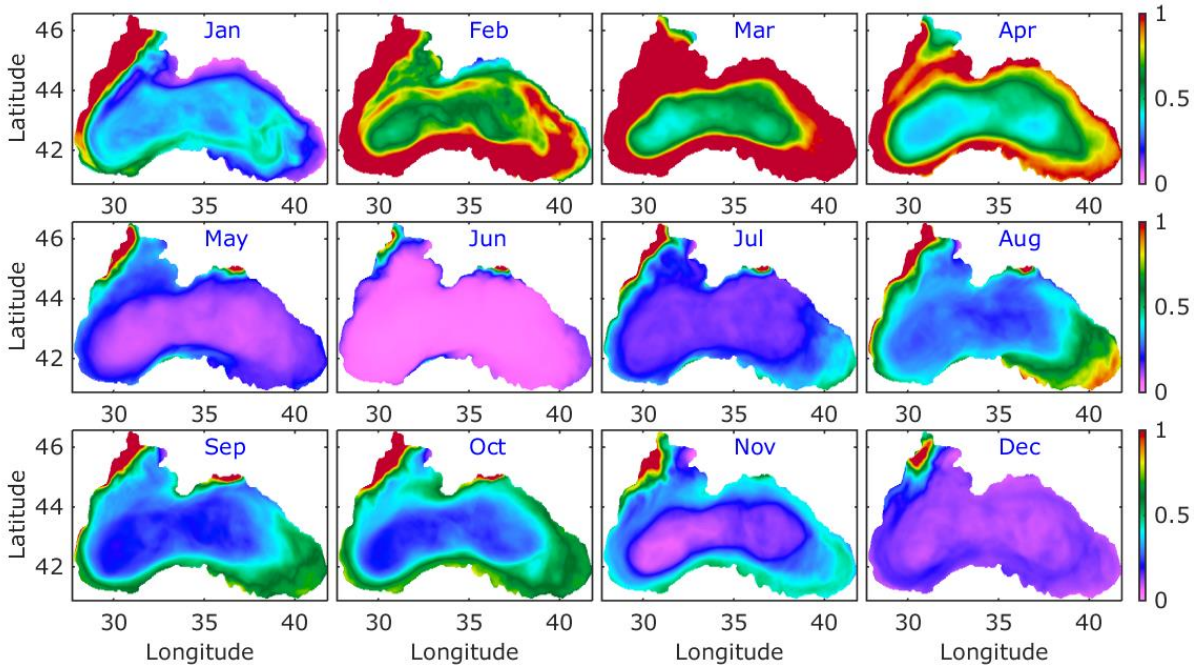

Figure 7. Climatological monthly distribution of phytoplankton (mmol N m^{-3}) from 2001 to 2010 (simulation with a river nutrient load).

Seasonal changes of the surface nitrate are illustrated in Fig. 6, where monthly mean values from 2001 to 2010 are extracted at 10 m depth. Typically, in winter (November-February), nutrient stocks in the surface waters are renewed from below the nutricline through upwelling, vertical diffusion, seasonal wind and buoyancy-induced entrainment processes, and later depleted by biological consumption. From April to September the nitrate is almost run down due to phytoplankton consumption. Predominantly, the lateral nitrate input comes from the Danube (Cociasu et al., 1996). The river influence markedly weakens toward the south along the coast and offshore for most of the year as a result of photosynthetic consumption. Nevertheless, the nutrient fluxes of anthropogenic origin are transported across the shelf and around the basin through the Rim Current system, and supplied ultimately to the interior basin (Pakhomova et al., 2014; Mikaelyan et al., 2014; Dorofeev, et al., 2013). In Fig. 7 the climatological (small + large) phytoplankton over 2001-2010 is shown. The phytoplankton in the surface layer, which is outside the area enclosed by the Rim current peaks in March, while in the deep basin interior the highest bloom is simulated in February. It is worth to note that the North-Western Shelf area is filled by elevated levels phytoplankton. Our simulations show early winter - spring bloom of the large phytoplankton (Figs. 7 and 8) that is in accordance with other modelling studies (Oguz et al., 1999 and 2001) and it is a specific characteristic of the annual plankton structure of the Black Sea ecosystem, which has been seen in every dataset irrespective of the top-down grazing control by top-predators (Sorokin, 2002; Vedernikov and Demidov, 1997). The large phytoplankton structure in the surface layer consists of two bloom events: in winter-spring and in fall. In winter, the maximum development of large phytoplankton is simulated, while in summer the small phytoplankton blooming is dominant. In summer, the large phytoplankton finds better growth conditions below the thermocline and above the halocline where nitrate concentrations are higher (Fig. 9). In summary, we can conclude that the model reproduces correctly the blooming periods (Vedernikov and Demidov, 1997) and the phytoplankton community succession.

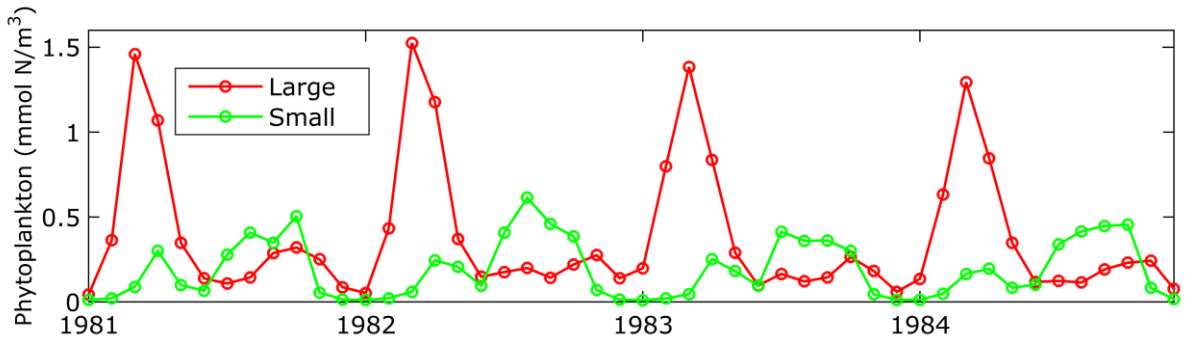

Figure 8. Monthly mean large and small phytoplankton (mmol N m^{-3}) averaged over the interior basin with depth greater than 200 m. Mean values from the surface to 10 m depth from the run with a nutrient load.

As a typical example of the water column distribution of nitrate and chlorophyll in the Black Sea interior, the deep basin average climatological profiles are shown in Fig. 9. These climatological profiles consist of twenty-year simulation from 1980 to 1999, which are produced without nutrient loads neither from rivers nor from atmosphere. The chlorophyll is calculated as the sum of small and large phytoplankton which is converted from (mmol N m^{-3}) to (mg Chl m^{-3}). It may depend on the fact that the Redfield ratio itself is a macroscopic property, being an empirical statistical average and not a fundamental biochemical constraint (Li, 2007). Phytoplankton species differ considerably in elemental composition, and the Redfield ratio results from an appropriate mix of stoichiometric types. We assume that the stoichiometric conversion of N to Chl - (mmol N m^{-3}):(mg Chl m^{-3})=1, and it remains unchanged despite the existing complexity.

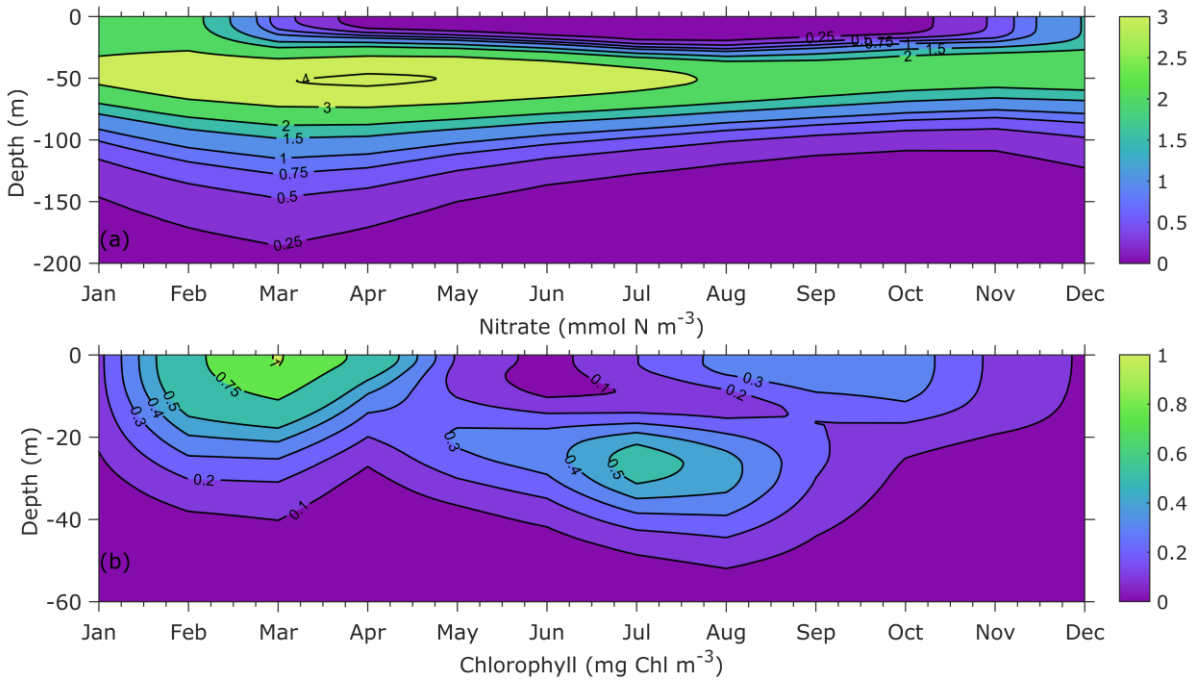

Figure 9. Monthly mean climatology of: (a) nitrate (mmol N m^{-3}) and (b) chlorophyll (mg Chl m^{-3}) averaged over the interior basin with depth greater than 200 m from the surface to 200 and 60 m depth, respectively. The twenty-year simulation (1980-1999) is performed without river nutrient load.

The upper mixed layer (ML) is scarce in nitrate for most of the year except for vertical winter mixing and occasional intrusion from coastal regions. Below ML nitrate concentration rises, forming a so-called upper nutricline zone (Gregg and Yakushev, 2005; Murray 2006), which is a portion of CIL, and supports summer subsurface production of large phytoplankton. There, nitrate attains maximum mean concentrations around 4 mmol N m^{-3}, and is re-supplied to the surface layer to refuel the biological pump. In winter, nitrate in the ML is renewed primarily from the upper part of the halocline through vertical diffusion, buoyancy induced mixing and upwelling, and depleted by biological utilisation. The large part of particulate organic matter is remineralised inside ML and the subsequent 10 – 20 m part of oxygenated zone. Only a small part of detritus particles sink to deeper anoxic part of the sea - about 100 -150 m depth (Fig. 9a). Karl and Knauer, 1991 reported that this depth is shallower in the sea interior (about 100 m) and about 200 m in the onshore, anticyclonically dominated zones. This conclusion is supported by our simulations since the results presented in Fig. 9 are extracted from both cyclonic and anticyclonic zones. It is worth to note that the simulated nitrate is within the range of measured and calculated values (Cannaby et al, 2015; Tugrul et al., 2014; Stanev et al., 2014).

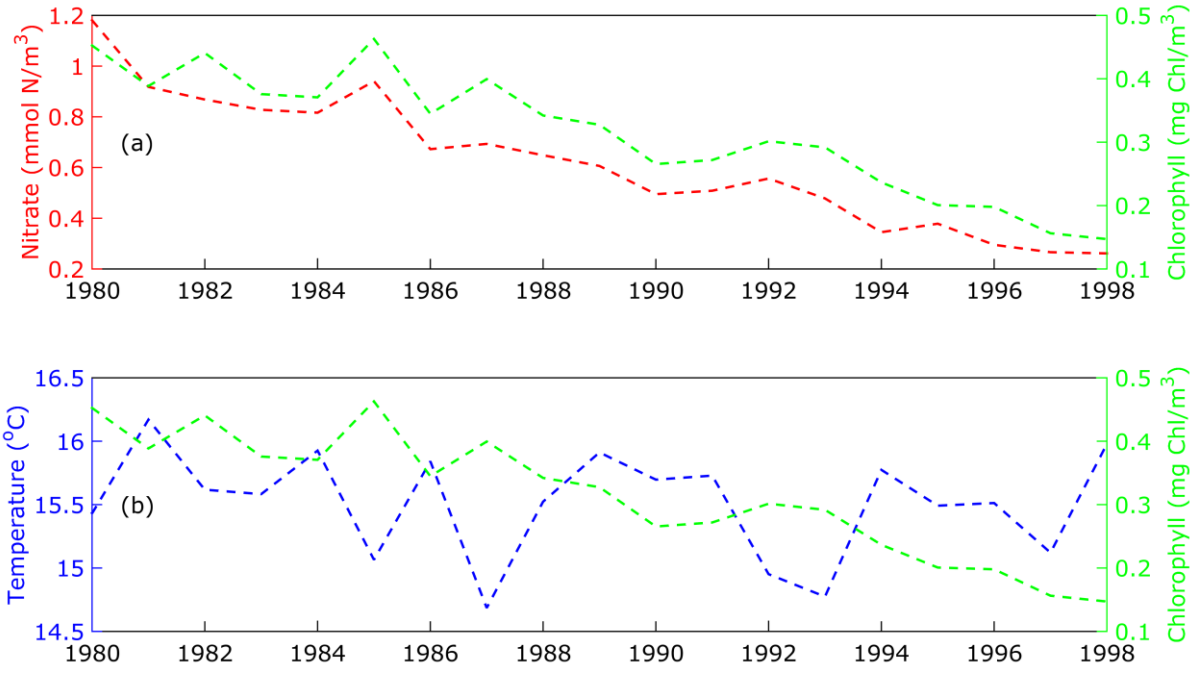

Figure 10. Time series of annual surface nitrate (mmol N m^{-3}), temperature (°C) and chlorophyll (mg Chl m^{-3}) averaged over the interior basin with depth greater than 200 m. Twenty-year simulation (1980-1999) is performed without river nutrient load.

Time series of annual nitrate (mmol N m^{-3}), temperature (°C) and chlorophyll (mg Chl m^{-3}) averaged over the interior basin with depth greater than 200 m are shown in Fig. 10. In the Black Sea deep basin, an increase in chlorophyll accompanies an increase in surface nitrate on the annual time scales (Fig. 10 a). The simulation is not forced with nutrient load from rivers and the variables are extracted at 2 m below the surface. The availability of nutrients to phytoplankton is mostly determined by effective mixing of the large pool of nutrient-rich water from depth because of lack of anthropogenic enrichment from rivers. Note, the negative correlation between the annual mean surface temperature and the chlorophyll yield until 1994 (Fig.10 b). Low surface temperature is usually associated with cold winters, which are accompanied by strong north-western and north-eastern winds. The wind is known to be a key factor in the formation of near

sea surface currents and, in particular, northerly winds over the Black Sea support basin cyclonic motion (Miladinova et al., 2016a). In the deep basin, annual average chlorophyll is linked to the mean surface temperature, which is an indicator of vertical stratification.

Due to the lack of consistent observational data for the 3D distribution of the BSEM state variables, the model is validated against satellite observations and independent simulations of the surface chlorophyll (http://marine.copernicus.eu). Monthly surface chlorophyll concentration from multi satellite observations (SeaWiFS, MODIS-Aqua and MERIS) available from the Copernicus Marine Environment Monitoring Service (CMEMS, http://marine.copernicus.eu) for 2000 is shown in Fig. 11. Further all results downloaded from CMEMS will be cited as CMEMS data. The data is reprocessed (Kopelevich et al., 2013) in order to eliminate data voids.

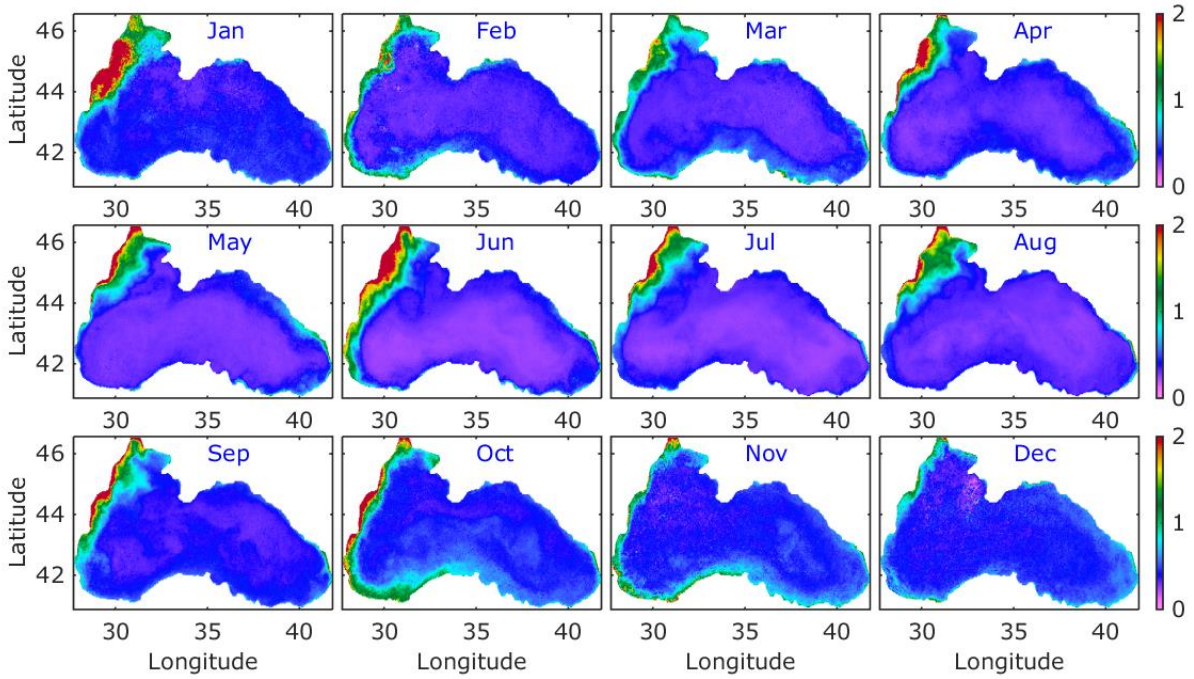

Figure 11. Monthly mean distribution of chlorophyll (mg Chl m^{-3}) from multi-satellite CMEMS reanalysis data for 2005.

The seasonal evolution of the surface chlorophyll in 2000 estimated by GETM-BSEM model is displayed in Fig. 12. Our simulations show a strong February-April spring surface bloom of phytoplankton followed by a lower bloom in summer-fall. These occurrences are in accordance with other modelling studies and observational data (Oguz et al., 1999 and 2001; Vedernikov and Demidov, 1997).

In winter-spring, the maximum development of phytoplankton is simulated in the North-Western Shelf, western and north-eastern coasts and along the Anatolian coast, as well as in the anticyclonic regions where the nitrate concentration is higher. The phytoplankton development intensifies in February and last till the beginning of May. In this particular year the summer bloom starts in August, however in other years it usually starts in July. The largest phytoplankton bloom was simulated for the peripheral area since the nutrient load coming from the rivers are distributed by the Rim jet and mixed by permanent or quasi-permanent anticyclonic eddies between the Rim current and the shelf. The formation of the seasonal thermocline beginning in March restricts the source of nitrate from nitricline and the biomass production is concentrated in the ML resulting in nitrate depletion.

Comparison between Figs. 11 and 12 shows that the GETM-BSEM shows stronger blooms than the satellite data. Both data sets indicate intensified chlorophyll production in the western, north-eastern coasts and along the Anatolian coast.

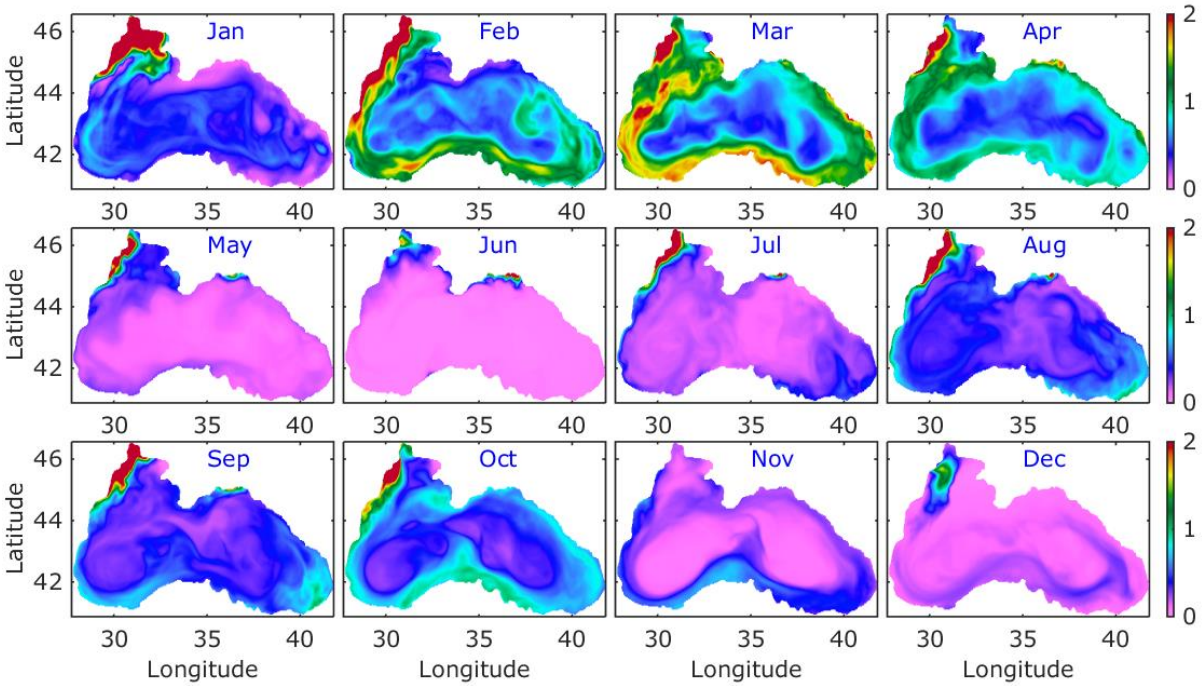

Figure 12. Monthly mean distribution of chlorophyll (mg Chl m^{-3}) in the surface 10 m for 2005 (GETM/BSEM simulation with river nutrient load).

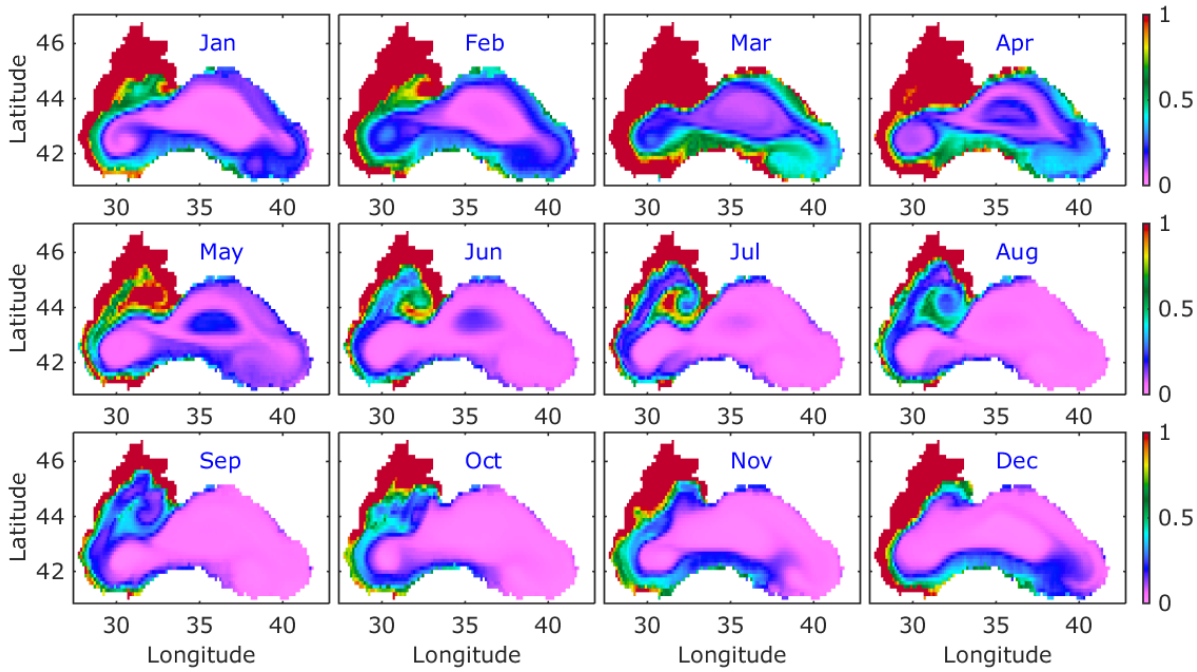

Figure 13. Monthly mean distribution of chlorophyll (mg Chl m^{-3}) in the surface 12 m for 2005 (simulations from CMEMS).

For further comparison, in Fig. 13 is shown again the surface chlorophyll in 2005, however, it consists of biogeochemical reanalysis for the Black Sea downloaded from CMEMS. The reanalysis for the Black Sea is produced by the MAST/ULg Production Unit by means of the GHER 3D circulation model online coupled with the BAMHBI biogeochemical model (Capet et al, 2016). CMEMS simulations support our finding that the North-Western Shelf chlorophyll concentrations are higher than the satellite concentrations (Fig. 11).

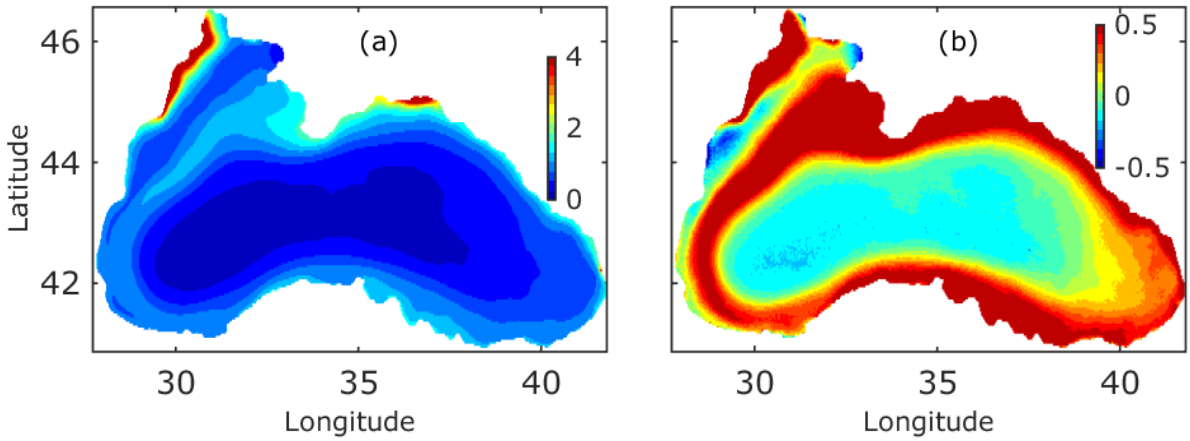

Figure 14. (a) Climatological mean chlorophyll (mg Chl m^{-3}) over 2001 – 2010. (b) Bias between GETM-BSEM model and CMEMS satellite climatology.

Climatological annual mean chlorophyll formed from monthly mean values is shown for illustration of the overall chlorophyll distribution in the entire basin (Fig. 14 a). For the spatial distribution of chlorophyll in the Black Sea, the most noticeable characteristic is its lower concentrations in the Rim current interior than in the exterior for all seasons. It is worth to note the higher chlorophyll in the Danube and Dniestr nearby zones and close to the Kerch Strait. The multi-annual (2001 – 2010) mean chlorophyll from multi-satellite CMEMS reanalysis, interpolated on the GETM domain, is extracted from the simulated multi-annual mean chlorophyll averaged over the same period (Figure 14 b). When model simulations are compared with the CMEMS satellite data, the BSEM model usually gives a bias of about 0.5 mg Chl m^{-3} in the northern and southern shelf areas, as well as along Rim current meandering in the western basin. Here it is notable that the bias in the interior is almost negligible.

4. Conclusions

The regional BSEM model has been applied for the first time for biogeochemical simulations of the Black Sea ecosystem. The BSEM model is able to describe the Black Sea specific features as demonstrated by the analysis presented herein. One of the key modification of the existing models is the introduction of two new components - the carnivore predators *Mnemiopsis* and *Noctiluca shunt.* Originally they began to exist in the lower trophic Black sea food web since the 80s. They feed on zooplankton and are responsible for the reduction of zooplankton standing stock that represents an ecological concern.

The model is coupled to the GETM hydrodynamic model. It is forced with fluxes, obtained from realistic meteorological conditions and tuned for the Black Sea ecosystem in particular. The main advantage of the GETM-BSEM model set-up for the Black Sea is the possibility to study: (i) the long-term evolution of the Black Sea ecosystem; (ii) the effect of nutrient load and regional weather on the biogeochemical structure.

The coupled model is able to capture basic physical and biological processes affecting phytoplankton variability and presents a good agreement with available data and model studies. Areas near the Danube plume and along the western Black sea coast and shelf are characterised by relatively high production throughout the year due to the continuous supply of nutrients by river discharge (primarily by Danube and also by Dniepr and Dniestr) and additionally due to the increased stratification caused by the low salinity zone. The Danube influenced area is clearly identified in the satellite chlorophyll images and the simulated phytoplankton especially during summer when nutrient supply from the deep waters is limited and Danube provides the main nutrient supply. In the absence of any physical mechanism to efficiently supply these inorganic nutrients into the euphotic zone, eutrophication could not play effective role in biological production throughout the entire basin, except coastal regions.

Despite that the North-Western Shelf area is rich in nutrients, this contribution is not the main source of nutrients in the deep sea area. Nitrate load from rivers is mainly spreading and circulating along the Rim current. The dynamical processes necessary to supply nutrients into the surface layer are generated by the strong wind stress forcing and intense cooling in the region, which subsequently lead to strong convective mixing in the water column to bring the nutrients from its subsurface pool. Therefore, the changing climatic forcing introduced an efficient mechanism, which intensified the anthropogenically-driven biogeochemical processes during the 80s. It is found that the vertical flux of nutrients from the pycnocline in winter is a key factor for phytoplankton growth in the sea interior and supports new production. Conversely, without appreciable subsurface nutrient accumulation in the absence of the eutrophication, strong vertical advective and convective processes in the water column might not be so effective for generating strong biological production in the basin. Consequently, the ecosystem conditions observed in the Black Sea in the recent 3-4 decades could be interpreted as the result of the joint process of anthropogenic and natural climatic forcing.

Appendix A. BSEM model equations

The general form of equations governing the biogeochemical model is expressed by

$$\frac{\partial(X \cdot H)}{\partial t} + \nabla\left[\vec{u} \cdot (X \cdot H)\right] = F_X + R_X$$

where X denotes each of the state variables, $\boldsymbol{u}$ is the three dimensional fluid velocity, $H = h + \eta$ the total water depth with h defining the bottom topography and η the surface elevation, F_X denotes the sum of horizontal and vertical diffusion terms, and R_X refers to the source-sink terms as described in a general form

$$R_X = Growth - Grazing - Excretion - (Respiration + Mortality)$$

Except R_X, the mathematical forms of all terms in the differential equation above and their numerical solution procedures are similar to those of the temperature and salinity transport equations in the GETM. GETM solves 3D transport equations for 11 non-conservative substances that BSEM involves. Detailed representation of source-sink terms is described below for each model compartment.

A.1. The autotrophs

Temporal variations of the large (P_L) and small (P_S) phytoplankton biomass are governed by the biological source-sink terms of the form

$$R_{PX} = \sigma_X \cdot \Psi_X \cdot P_X - \sum G(P_X) \cdot Z_X - m_{PX} \cdot P_X \qquad \text{(A1a)}$$

where

$$\Psi_X = f_X(N_n, N_a) \cdot f_X(I) \cdot f_X(T) \qquad \text{(A1b)}$$

represents the total limitation function of the primary production, and the subscript X denotes either L for the large or S for the small size group. The right hand side of eq. A1a describes, respectively, the phytoplankton growth (primary production), grazing by different zooplankton groups, and physiological mortality that also includes the respiration. This simplification is justified in the absence of explicit representation of the microbial loop. The phytoplankton growth is modelled as the product of phytoplankton biomass P and the maximum specific growth rate σ. The growth, however, is subject to simultaneous limitations by the availability of nitrogen resource $f(N_n,N_a)$, the photosynthetically available radiation $f(I)$, and temperature $f(T)$. Using a spectrally unresolved model, the light limitation is parameterized by (Jassby and Platt, 1976)

$$f_X(I) = \tanh\left[\alpha_X \cdot I\right] \cdot e^{-\beta_X I} \qquad \text{(A2a)}$$

$$I = I_S \cdot \exp\left\{-\mathrm{k_w z} - \int_0^z k_b(\mathrm{P_L} + \mathrm{P_S} + \mathrm{D}) \cdot dz\right\} \qquad \text{(A2b)}$$

where α_X is a parameter controlling slope of the photosynthesis-irradiance curve at low values of the photosynthetically available irradiance (PAR) whose surface intensity I_S amounts to half of the incoming solar radiation, β_X is the photoinhibition parameter to reduce the growth at high irradiance conditions. The light attenuation below the sea surface is represented by an exponential decay function in which the total light extinction coefficient k comprises the contributions from sea water itself (k_w), and self-shading effects of phytoplankton and detritus material (k_b); $k = k_w + (P_L + P_S + D)k_b$.

The nitrogen limitation function comprises the sum of individual contributions of the ammonium and nitrate limitations; $f_X(N_n,N_a) = f_X(N_n) + f_X(N_a)$. They are expressed by the Monod-type hyperbolic functions involving a saturation response at high resource concentrations

$$f_X(N_a)=\left[\frac{N_a}{K_{AX}+N_a}\right] \quad \text{and} \quad f_X(N_n)=\left[\frac{N_n}{K_{NX}+N_n}\right]\cdot\left[\frac{K_{AX}}{K_{AX}+N_a}\right] \qquad \text{(A3a,b)}$$

where N_a and N_n denote ammonium and nitrate concentrations, respectively; K_{AX} and K_{NX} are the corresponding half saturation constants of ammonium and nitrate uptakes. The term within the second square brackets of eq. A3b represents the ammonium limitation of the nitrate uptake due to preferred consumption of ammonium in the growth process. The silicate control on the diatom growth is neglected as the available data does not yield evidence for the prevailing role of silicate limitation although its input from major rivers tends to decline during the last two decades. The temperature control of the form

$$f_L(T)=Q_{10}^{(12-T)/12} \qquad \text{(A3c)}$$

is imposed for the growth of large phytoplankton group to promote its growth at low temperatures and to reduce at high temperatures. No temperature control is imposed for the small phytoplankton group, but lower growth rate of the large phytoplankton group at high temperatures gives indirectly the small phytoplankton group a growth advantage.

A.2. The heterotrophs and carnivores

Changes in the zooplankton biomass are controlled by ingestion, predation, excretion, and mortality which are expressed by

$$R(Z_S)=\gamma_Z G_S(P_S)Z_S-\left[G_L(Z_S)Z_L+G_N(Z_S)Z_N+G_G(Z_S)Z_G\right]-\mu_S Z_S-m_S Z_s^2 \qquad \text{(A4a)}$$

$$R(Z_N)=\gamma_Z\left[G_N(P_L)+G_N(Z_S)+G_N(D_n)\right]Z_N - G_L(Z_N)Z_L-G_G(Z_N)Z_G-\mu_N Z_N-m_N Z_N^2 \qquad \text{(A4b)}$$

$$R(Z_L)=\gamma_Z\left[G_L(P_L)+G_L(Z_S)+G_L(Z_N)+G_L(D_n)\right]Z_L - G_G(Z_L)Z_G-\mu_L Z_L-m_L Z_L^2 \qquad \text{(A4c)}$$

$$R(Z_G)=\gamma_Z\left[G_G(Z_S)+G_G(Z_L)+G_G(Z_N)\right]Z_G-\mu_G Z_G-m_G\cdot Q_{10}^{(15-T)/5}\cdot Z_G^2 \qquad \text{(A4d)}$$

where the subscript *G* denotes the *Mnemiopsis* zooplankton group and *N* - the *Noctiluca* group, and γ_Z, μ_X and m_X are, respectively, the coefficient of assimilation efficiency, the excretion rate and the natural mortality rate expressed in the quadratic form.

The ingestion terms within the square brackets are represented by the Michaelis-Menten (the so-called Holling type II) functional form in terms of the maximum rate g_j, the temperature limitation function $f_j(T)$, and the food capture efficiency coefficient $b_{j,i}$ for the food item X_i by

$$G_j(X_i)=g_j f_j(T)\frac{b_{j,i}\cdot X_i}{K_j+\left[\sum_i b_{j,i}\cdot X_i\right]} \qquad \text{(A5a)}$$

where the terms within the square bracket in the denominator refer to the total food available for the consumption of any zooplankton group, and K_j denotes its half-

saturation value. The food preference coefficients are expressed as a function of the relative proportion of the total food by

$$b_{j,i} = \frac{a_{j,i} \cdot P_i}{\sum_i a_{j,i} \cdot P_i} \qquad \text{(A5b)}$$

where $a_{j,i}$ denotes the constant food preference coefficient specified externally as in Table A1. According to eq. A5a,b, when a food type declines, its grazing preference decreases (Gentleman et al., 2003) . In this case, zooplankton select an alternative food type having higher biomass. Thus, grazing preferences may switch from one prey to another depending on local conditions and the predator may select temporally and spatially most favourable food types.

The temperature control of the growth, $f_j(T)$, is introduced for the *Noctiluca* and the gelatinous group *Mnemiopsis* in the form

$$f_{ZN}(T) = Q_{10}^{(T-12)/8} \qquad \text{(A6a)}$$

$$f_{ZG}(T) = Q_{10}^{(T-20)/4} \quad for \quad T > 20 \quad and \quad f_{ZG}(T) = 1 \quad otherwise \qquad \text{(A6b)}$$

According to the observations, *Noctiluca* can maintain its growth at a wide temperature range of 12-30°C. Eq. A6a supresses the *Noctiluca* growth at low temperatures but favours it in spring and summer months when the surface mixed layer starts warming up. Eq. A6b imposes the growth advantage of *Mnemiopsis* population at high temperatures during July-August.

A.3. Particulate organic nitrogen (PON)

Egestion and sloppy feeding (i.e. unassimilated part of the food grazed) given by eq. A7a and phytoplankton and zooplankton mortalities in eq. A7b form the detritus sources. Its consumption by zooplankton groups within the water column (eq. A7c) and transformation into the dissolved organic nitrogen pool at a rate ε_n constitutes the sinks of detritus.

$$\begin{aligned} DETR1 = {} & (1-\gamma_Z)G_S(P_S)Z_S + (1-\gamma_Z)[G_N(P_L) + G_N(Z_S)]Z_N \\ & + (1-\gamma_Z)[G_L(P_L) + G_L(Z_S) + G_L(Z_N)]Z_L \\ & + (1-\gamma_Z)[G_G(Z_S) + G_G(Z_L) + G_G(Z_N)]Z_G \end{aligned} \qquad \text{(A7a)}$$

$$DETR2 = \left[\sum_k m_{Pk} P_k + \sum_k m_k Z_k^2\right] \qquad \text{(A7b)}$$

$$DETR3 = \gamma_Z \cdot [G_L(D_n)Z_L + G_N(D_n)Z_N] \qquad \text{(A7c)}$$

The total source-sink terms for the detritus equation is given by

$$R(D_n) = DETR1 + DETR2 - DETR3 - \varepsilon_n D_n \qquad \text{(A7d)}$$

Following the chemical reactions in Eq. 12a-c, the decomposition rate of particulate organic nitrogen is represented by

$$\varepsilon_n(DO) = \varepsilon_{n0}\left[1 + \frac{R_0}{R_0 + DO}\right] \quad for \quad DO < 250\mu M$$

$$\varepsilon_n(DO) = \varepsilon_{n0} \quad otherwise \qquad \text{(A7e)}$$

which implies twice higher decomposition rate in the oxygen deficient part of the water column due to more active bacterial processes with respect to the surface aerobic layer.

A.4. Dissolved inorganic nitrogen (DIN)

The changes in ammonium and nitrate concentrations are expressed by

$$R(N_a) = \varepsilon_n D_n + \sum_k \mu_{zk} \cdot Z_k - \left[\sum_k \sigma_k \cdot f_k(T) \cdot f_k(I) \cdot f_k(N_a) \cdot P_k \right] - r_n \cdot N_a - r_a \cdot N_a \cdot N_n - r_b \cdot N_a \quad \text{(A9a)}$$

$$R(N_n) = r_n \cdot N_a - \left[\sum_k \sigma_k \cdot f_k(T) \cdot f_k(I) \cdot f_k(N_n) \cdot P_k \right] - 0.8 \cdot \varepsilon_n \cdot D_n - \frac{3}{5} r_a \cdot N_a \cdot N_n - \frac{4}{3} r_s \cdot HS \cdot N_n \quad \text{(A9b)}$$

In eq. A9a, the first and second terms represent ammonium sources due to decomposition of PON and zooplankton excretion, respectively. The third term represents its uptake during the primary production and the last two terms are the ammonium oxidation by oxygen and nitrate following the reactions in Eqs. A13a,b. According to eq. A9b, the only internal source of nitrate is its recycled form due to the oxidation of ammonium (the first term). Nitrate concentration is consumed due to its uptake (the second term), anaerobic particulate matter remineralization following eq. A12b (the third term) that applies at oxygen concentrations less than *10* mmol O_2 m^{-3}, the oxidations of ammonium and hydrogen sulphide taking place at oxygen concentrations less than *20* mmol O_2 m^{-3} following equations A13b,d.

A.5. Dissolved oxygen and hydrogen sulphide

Dissolved oxygen concentration is altered by a balance between its photosynthetic production by the autotrophs and the consumption due to the pelagic decomposition of organic matter (eq. A12a). The excretion of zooplankton as well as the oxidation of ammonium (eq. A13a) within the oxygenated parts of the water column (O_2 > 10 mmol O_2 m^{-3}) and oxidation of hydrogen sulphide near the anoxic interface (eq. A13d), as given by

$$R(DO) = 8.125 \left[\sum_k \Psi_k \cdot P_k \right] - 6.625 \left[\varepsilon_n \cdot D_n + \sum_k \mu_{zk} \cdot Z_k \right] - 2 r_n \cdot N_a - \frac{1}{2} r_o \cdot HS \cdot DO \quad \text{(A11a)}$$

The air-sea exchanges of surface dissolved oxygen concentration is given by

$$K_v \frac{\partial DO}{\partial z} = -V_p \cdot \left[DO_{sat} - DO(z=0) \right] \quad \text{(A11b)}$$

where K_v is the vertical diffusivity, DO_{sat} represents the oxygen saturation concentration computed according to the UNESCO formula (1996) , and V_p is the gas transfer velocity computed according to the relation given by Wanninkhof (1992).

The reaction kinetics governing temporal changes of hydrogen sulphide concentration are given by

$$R(HS) = 0.5 \cdot \varepsilon_n \cdot D_n - r_o \cdot HS \cdot DO - r_s \cdot HS \cdot N_n - r_u \cdot HS \quad \text{(A11c)}$$

where the first term represents hydrogen sulphide production by the process of sulphate based anaerobic organic matter decomposition (Eqs. A12c), the second and third terms express the oxidation reactions of H_2S by oxygen and nitrate (Eqs. A13c,d), respectively.

A.6. Redox reactions

The organic matter is decomposed in different parts of the water column following the reactions

$$OM + 130O_2 = xCO_2 + yNH_3 + H_3PO_4 + xH_2O$$

$$OM + 0.8 * xHNO_3 = xCO_2 + yNH_3 + H_3PO_4 + 1.4 * xH_2O + 0.4 * xN_2$$

$$OM + 0.5 * xSO_4^{2-} = xCO_2 + yNH_3 + H_3PO_4 + 0.5 * xH_2S$$

where

$$OM = (CH_2O)_x (NH_3)_y H_3PO_4 \qquad \text{(A12a-d)}$$

and x=106 and y=16 denote the Redfield stoichiometric coefficients for the molar C:P and N:P ratios, respectively. For more extensive description of the stoichiometry of remineralisation and denitrification processes, we refer to Paulmier et al. (2009).

Ammonium is oxidized by oxygen within the aerobic part of the water column to form the dissolved inorganic nitrate (i.e. the nitrification process). It is also oxidized by nitrate within the suboxic zone to prevent its upward flux from the anoxic pool into the euphotic zone. The reactions for these processes are given by

$$NH_4 + 2O_2 = NO_3 + 2H^+ + H_2O \qquad \text{(A13a)}$$

$$NH_4 + 3/5NO_3 = 4/5N_2 + 9/5H_2O + 2/5H^+ \qquad \text{(A13b)}$$

Hydrogen sulphide is oxidized near the anoxic interface by oxygen and nitrate following the reactions

$$H_2S + \frac{1}{2}O_2 = S^0 + H_2O \qquad \text{(A13c)}$$

$$H_2S + 4/3NO_3 + 2OH^- = SO_4^{2} + 2/3N_2 + 2H_2O \qquad \text{(A13d)}$$

Table A1. Food capture efficiency parameters of the zooplankton groups

	Microzooplankton	Mesozooplankton	*Noctiluca*	*Mnemiopsis*
Large phytoplankton	--	1.0	0.5	--
Small phytoplankton	1.0	--	0.5	--
Detritus	--	0.5	1.0	--
Microzooplankton	--	0.5	0.25	1.0
Mesozooplankton	--	--	--	0.5
Noctiluca	--	0.25	--	0.3

Appendix B. BSEM input parameters

Recently, several parameters concerning phytoplankton growth, respiration, mortality and excretion rates have been updated that enabled a better consistence of simulations with the observations. All model parameters and their values used in the present study are given in Table B1.

Table B1. BSEM input parameters as they are listed in the "fabm.yaml" FABM input file.

Parameter	Value	Unit	Definition	Default
sfl_ni	0.0	mmol $Nm^{-2}d^{-1}$	Constant surface nitrate flux	0.083
sfl_am	0.0	mmol $Nm^{-2}d^{-1}$	Constant surface ammonium flux	0.0225
pl0	0.0225	mmol N m^{-3}	Minimum large phytoplankton concentration	0.0225
ps0	0.0225	mmol N m^{-3}	Minimum small phytoplankton concentration	0.0225
alpha_l	0.4	-	Initial slope of P-I curve for large phytoplankton	0.8
alpha_s	0.2	-	Initial slope of P-I curve for small phytoplankton	0.35
sigma_l	1.2	d^{-1}	Maximum growth rate large phytoplankton	1.2
sigma_s	1.0	d^{-1}	Maximum growth rate small phytoplankton	1.0
beta_l	0.0015	-	Photoinhibition parameter for large phytoplankton	0.0015
beta_s	0.35	-	Photoinhibition parameter for small phytoplankton	0.35
kb	0.01		Self-shading attenuation	0.01
ka_l	0.3		Half-saturation constant for ammonium uptake from large phytoplankton	0.3
ka_s	0.2		Half-saturation constant for ammonium uptake from small phytoplankton	0.2
kn_l	0.5		Half-saturation constant for nitrate uptake from large phytoplankton	0.5
kn_s	0.3		Half-saturation constant for nitrate uptake from small phytoplankton	0.3
mpl	0.05	d^{-1}	Mortality rate for large phytoplankton	0.005
mps	0.06	d^{-1}	Mortality rate for small phytoplankton	0.006

Parameter	Value	Unit	Definition	Default
Q10	2.0		Factor of temperature control	2.
phyZ	0.7		Zooplankton assimilation efficiency	0.7
g_zs	0.8	d^{-1}	Maximum grazing rate of small zooplankton	0.8
g_zl	0.5	d^{-1}	Maximum grazing rate of large zooplankton	0.5
g_zn	0.5	d^{-1}	Maximum grazing rate of *Noctiluca*	0.5
g_zg:	0.15	d^{-1}	Maximum grazing rate of *Mnemiopsis*	0.5
k_zs	0.4		Half-saturation constant for grazing of small zooplankton	0.4
k_zl	0.5		Half-saturation constant for grazing of large zooplankton	0.5
k_zn	0.4		Half-saturation constant for grazing of *Noctiluca*	0.4
kn_zg	0.25		Half-saturation constant for grazing of *Mnemiopsis*	0.25
mzs	0.1	d^{-1}	Mortality rate of small zooplankton	0.1
mzl0	0.25	d^{-1}	Default mortality rate of large zooplankton	0.25
mzn	0.15	d^{-1}	Mortality rate of *Noctiluca*	0.15
mnzg	0.02	d^{-1}	Mortality rate of *Mnemiopsis*	0.02
mpzg0	0.1	d^{-1}	Default predation mortality rate of *Mnemiopsis*	0.1
mu_zs	0.06	d^{-1}	Excretion rate of small zooplankton	0.06
mu_zl	0.05	d^{-1}	Excretion rate of large zooplankton	0.05
mu_zn	0.06	d^{-1}	Excretion rate of *Noctiluca*	0.06
mu_zg	0.08	d^{-1}	Excretion rate of *Mnemiopsis*	0.08
epsilon_n0	0.01	d^{-1}	Default remineralisation rate of detritus	0.05
R0	150.0		Half-saturation constant for detritus remineralisation	150.0
w_dn	5.0	m d^{-1}	Detritus sedimentation rate	5.0
r_n0	0.1	d^{-1}	Default nitrification rate	0.1
r_a0	0.01	d^{-1}	Default ammonium oxidation rate by	0.1

Parameter	Value	Unit	Definition	Default
			nitrate	
r_s	0.01	d^{-1}	HS oxidation rate by nitrate	0.1
r_o	0.01	d^{-1}	HS oxidation rate by oxygen	0.1
r_u	0.000	d^{-1}	HS oxidation rate by other processes	0.1
s1	5.3		Reduced nitrate/oxidized detritus	5.3
s2	6.625		Oxygen production/recycled nitrogen	6.625
s4	2.0		Nitrification	2
lds	3.5	m d^{-1}	Rate of detritus sinking into sediment	3.5
lsd	25.0	d^{-1}	Rate of sediment resuspension	25.0
tau_crit	0.07	**N**m^{-2}	Critical bottom stress	0.07
lsa	0.001	d^{-1}	Rate of sediment mineralisation	0.001
bsa	0.15	$°C^{-1}$	Temperature control of sediment mineralisation	0.15
pvel_c	4.5	-	A constant to adjust the oxygen flux	4.5
temp_bio_high	20.0	°C	Upper temperature control of biological reactions	20.0
temp_bio_low	5.0	°C	Lower temperature control of biological reactions	5.0
par_lim	75.0	W m^{-2}	PAR limitation for photo inhibition	75.0
temp_zg_lim	16.0	°C	*Mnemiopsis* critical temperature	16.0
ox_zoop_grazing	200.0	mmol O_2 m^{-3}	Oxygen control for zooplankton grazing	200.0
ox_min	0.05	mmol O_2 m^{-3}	Oxygen minimum allowed value	0.05
ox_lim_exc	300.0	mmol O_2 m^{-3}	Oxygen control for zooplankton excretion	300.0
ox_suboxic	10.0	mmol O_2 m^{-3}	Oxygen control for suboxic conditions	10.0
zl_pred_lost	0.5	-	Fraction of the large zooplankton lost by predation	0.5
Initialization				
pl	0.0045	mmol N m^{-3}	Large phytoplankton	
ps	0.0045	mmol N m^{-3}	Small phytoplankton	
zs	0.0025	mmol N m^{-3}	Small zooplankton	
zl	0.0025	mmol N m^{-3}	Large zooplankton	

Parameter	Value	Unit	Definition	Default
zn	0.0025	mmol N m^{-3}	*Noctiluca*	
zg	0.0025	mmol N m^{-3}	*Mnemiopsis*	
dn	0.07	mmol N m^{-3}	Detritus	
fl	0.0	mmol Nm^{-3}	Fluff	

References

Bruggeman, J. and Bolding, K. 2014. A general framework for aquatic biogeochemical models. Environmental Modelling and Software, 61, 249–265

Cannaby, H., Bettina A. Fach, Sinan S. Arkin, Baris Salihoglu, 2015. Climatic controls on biophysical interactions in the Black Sea under present day conditions and a potential future (A1B) climate scenario, Journal of Marine Systems 141, 149–166 doi:10.1016/j.jmarsys.2014.08.005

Capet A., Meysman, F., Akoumianaki, I., Soetaert, K. and Grégoire, M. 2016. Integrating sediment biogeochemistry into 3D oceanic models: A study of benthicpelagic coupling in the Black Sea. Ocean Modelling, 101, 83-100.

Cociasu, A., L. Dorogan, C. Humborg and L. Popa, 1996. Long-term ecological changes in the Romanian coastal waters of the Black Sea. Marine Pollution Bulletin, 32**,** 32–38.

Daskalov, G.M. Long-term changes in fish abundance and environmental indices in the Black Sea. *Marine Ecology Progress Series* 255:259-270. 2003

Dorofeev, V.L., Korotaev, G.K. & Sukhikh, L.I., 2013. Study of long-term variations in the Black Sea fields using an interdisciplinary physical and biogeochemical model, Izv. Atmos. Ocean. Phys. 49, 622-631. doi:10.1134/S0001433813060054

Garcia-Gorriz E., Macias Moy D., Stips A. and Miladinova-Marinova S. (2016) JRC Marine Modelling Framework in support of the Marine Strategy Framework Directive: Inventory of models, basin configurations and datasets. JRC Technical Report, EUR27885, doi:10.2788/607272

Garnier, J., G. Billen, E. Hannon, S. Fonbonne, Y. Vdenina and M. Soulie, Modeling transfer and retention of nutrients in drainage network of the Danube River. *Estuarine, Coastal and Shelf Science,* **54,** 285–308, 2002.

Gentleman, W., Leising, A., Frost, B., Strom, S. and Murray, J. (2003) Functional responses for zooplankton feeding on multiple resources: a review of assumptions and biological dynamics. Deep Sea Res. II, 50, 2847--2875.

Gregg, M.C. and Yakushev, E., Surface ventilation of the Black Sea's cold intermediate layer in the middle of the western gyre. Geophysical Research Letters 32, 2005. L03604. doi:10.1029/2004GL021580.

Gregoire, M., Nezlin, N., Kostianoy, A., and Soetaert, K.: Modeling the nitrogen cycling and plankton productivity in an enclosed environment (the Black Sea) using a three-dimensional coupled hydrodynamical – ecosystem model, J. Geophys. Res., 109, C05007, 2004.

Gregoire, M., Raick, C., and Soetaert, K.: Numerical modeling of the Central Black Sea ecosystem functioning during the eutrophication phase, Progr. Oceanogr., 76, 286–333, 2008.

He, Y., E. V. Stanev, E. Yakushev, J. Staneva: Black Sea biogeochemistry: Response to decadal atmospheric variability during 1960-2000 inferred from numerical modeling. Marine Environmental Research, 77, 90-102. (2012)

Jassby, A.D. and Platt, T., 1976. Mathematical formulation of the relationship between photosynthesis and light for phytoplankton. Liinnology and Oceanography, 21,540-547

Karl, D.M., and G.A. Knauer. Microbial production and particle flux in the upper 350 m of the Black Sea. Deep Sea Res., 38, Supp. 2A, S655-S661, 1991

Lancelot, C. , J. Staneva, D. Van Eeckhout, J. Beckers, E. Stanev, Modelling the Danube-influenced north-western continental shelf of the Black Sea. II: Ecosystem response to changes in nutrient delivery by Danube river after its damming in (1972),” Estuarine Coastal Shelf Sci., 54, 473–499, 2002

Li, W.K.W. 2007. Macroscopic patterns in marine plankton. Encyclopedia of Biodiversity, Elsevier. doi:10.1016/B978-012226865-6/00582-1.

Ludwig W, Bouwman AF, Dumont E, Lespinas F Water and nutrient fluxes from major Mediterranean and Black Sea rivers: Past and future trends and their implications for the basin - scale budgets, Global Biogeochem. Cycles, 24, GB0A13, (2010)

Mikaelyan, S. A., Zatsepin, A. G., Chasovnikov, V.K., 2013. Long-term changes in nutrient supply of phytoplankton growth in the Black Sea. Journal of Marine Systems, Vol. 117-118: 53–64

Miladinova S., A. Stips, E. Garcia-Gorriz, D. Macias Moy (2016a), Changes in the Black Sea physical properties and their effect on the ecosystem, EUR 28060, doi:10.2788/69832

Miladinova-Marinova S., A. Stips, E. Garcia-Gorriz, D. Macias Moy (2016b), Black Sea ecosystem model: setup and validation, EUR 27786, doi: 10.2788/601495

McQuatters-Gollop, A., Mee, L. D., Raitsos, D. E., and Shapiro,G. I.: Non-linearities, regime shifts and recovery: The recent influence of climate on Black Sea chlorophyll, J. Marine Syst.,74, 649–658, 2008.

Murray, J.W. (Ed.), Black Sea Oceanography. Deep-Sea Research II, vol. 53, pp. 1737–2004, 2006.

Oguz T., P.E. La Violette, Ü. Ünlüata: The upper layer circulation of the Black Sea: its variability as inferred from hydrographie and satellite observations. *J. Geophys. Res.,* 97, CS, 12569-12584, 1992.

Oguz, T., P., Malanotte-Rizzoli, D., Aubrey, Wind and thermohaline circulation of the Black Sea driven by yearly mean climatological forcing, J. Geophys. Res. 100, 6846–6865, 1995.

Oguz, T., H. Ducklow, P. Malanotte-Rizzoli, J.W. Murray, V.I. Vedernikov, and U. Unluata. A physical-biochemical model of plankton productivity and nitrogen cycling in the Black Sea. Deep-Sea Res. I. 46, 597–636 , 1999

Oguz, T., Ducklow, H.W., and Malanotte-Rizzoli, P.: Modeling distinct vertical biogeochemical structure of the Black Sea: dynamical coupling of the oxic, suboxic and anoxic layers, Global Biogeochem. Cy., 14, 1331–1352, 2000.

Oguz, T., H. W. Ducklow, J. E. Purcell, and P. Malanotte-Rizzoli. Modeling the response of topdown control exerted by gelatinous carnivores on the Black Sea pelagic food web. J. Geophys. Res., 106, 4543–4564, 2001

Oguz, T., Tugrul, S., Kideys, A.E., Ediger, V.and Kubilay, N.: Physical and biogeochemical characteristics of the Black Sea (28,S), in: The Sea, vol. 14, edited by: Robinson, A. R. and Brink, K. H., Harvard University Press, chap. 33, 1331–1369, 2004.

Oguz T, and Merico A: Factors controlling the summer *Emiliania huxleyi* bloom in the Black Sea: a modelling study. J Mar Syst 59:173–188, 2006.

Oguz T, Dippner JW, Kaymaz Z: Climatic regulation of the Black Sea hydro-meteorological and ecological properties at interannual-to-decadal time scales. J Mar Syst 60(3–4):235–254, 2006. doi:10.1016/j.jmarsys.2005.11.011.

Oguz, T., B. Salihoglu, and B. Fach, "A coupled plankton–anchovy population dynamics model assessing nonlinear controls of anchovy and gelatinous biomass in the Black Sea," Mar. Ecol. Prog. Ser. **369**, 229–256,2008.

Oguz, T., Stips, A., Macias, D., Garcia-Gorriz, E. and Coughlan, C.: Development of the Black Sea specific ecosystem model (BSSM), Technical report, EUR27003EN, European Commission, Ispra, 2014.

Pakhomova, S., E. Vinogradova, E. Yakushev, et al., "Interannual variability of the Black Sea proper oxygen and nutrients regime: the role of climatic and anthropogenic forcing," Estuarine, Coastal Shelf Sci. **140**, 134–145 (2014).

Paulmier, A., Kriest, I., and Oschlies, A.: Stoichiometries of remineralisation and denitrification in global biogeochemical ocean models, Biogeosciences, 6, 923–935, 2009, http://www.biogeosciences.net/6/923/2009/

Sorokin, Y.I., 2002. The Black Sea ecology and oceanography. Backhuys Publishers, Leiden, 875 pp.

Stanev, E., He, Y., Staneva, J. and Yakushev, E.: Mixing in the Black Sea detected from the temporal and spatial variability of oxygen and sulfide – Argo float observations and numerical modelling, Biogeosciences, 11, 5707–5732, 2014

Staneva, J., V. Kourafalou, and K. Tsiaras, 2010. Seasonal and Interannual Variability of the North-Western Black Sea Ecosystem. Terr. Atmos. Ocean. Sci., 21, 163-180.

Stips, A., Mark Dowell, Francesca Somma, Clare Coughlan, Chiara Piroddi, Faycal Bouraoui, Diego Macias, Elisa Garcia-Gorriz, Ana Cristina Cardoso, Giovanni Bidoglio, 2015. Towards an integrated water modelling toolbox. JRC EUR 92843.

Tugrul, S., Murray, J. W., Friederich, G. E., and Salihoğlu, I.: Spatial and temporal variability in the chemical properties of the oxic and suboxic layers of the Black Sea, J. Marine Syst., 135, 29–43, 2014.

Zatsepin, A. G., A. I. Ginzburg, A. G. Kostianoy, V. V. Kremenetskiy, V. G. Krivosheya, S. V. Stanichny, and P.-M. Poulain, Observations of Black Sea mesoscale eddies and associated horizontal mixing, J. Geophys. Res., 108(C8), 3246, doi:10.1029/2002JC001390, 2003.

Vedernikov, V.I. and A.B. Demidov, 1997. Vertical distributions of primary production and chlorophyll during different seasons in deep part of the Black Sea, Oceanology, 37**,** 376-384.

Yakushev, E. V., Pollehne, F., Jost, G., Kuznetsov, I., Schneider, B., and Umlauf, L.: Analysis of the water column oxic/anoxic interface in the Black and Baltic seas with a numerical model, Mar. Chem., 107, 388–410, 2007.

Wanninkhof, R. 1992. Relationship between gas exchange and wind speed over the ocean. J. Geophys. Res.,97, 7373-7381.

List of abbreviations and definitions

BSEM: Black Sea Specific Ecosystem Model
CIL: Cold Intermediate Layer
ECMWF: European Center for Medium Range Weather Forecast
ERA40: ECMWF ERA 40 reanalysis
ERA-interim: ECMWF ERA-interim reanalysis
ETOPO1: Earth topography database
EU: European Union
FABM: Framework for Aquatic Biogeochemical Models
GRDC: Global River Data Center database
GETM: General Estuarine Ocean Model
JRC: Joint Research Centre
MC: Marie Curie
ML: Mixed layer
MEDAR/MEDATLAS: Mediterranean Data Archaeology and Rescue database
MSFD: Marine Strategy Framework Directive
N: Nitrate
SIMSEA: Scenario simulations of the changing Black Sea ecosystem
SeaWiFS: Sea viewing Wide Field of view Sensor
HS: Hydrogen sulphide
SST: Sea surface temperature

List of figures

List of tables

Europe Direct is a service to help you find answers to your questions about the European Union.

Freephone number (*)**:**

00 800 6 7 8 9 10 11

(*) The information given is free, as are most calls (though some operators, phone boxes or hotels may charge you).

More information on the European Union is available on the internet (http://europa.eu).

HOW TO OBTAIN EU PUBLICATIONS

Free publications:

- one copy:
  via EU Bookshop (http://bookshop.europa.eu);
- more than one copy or posters/maps:
  from the European Union's representations (http://ec.europa.eu/represent_en.htm);
  from the delegations in non-EU countries (http://eeas.europa.eu/delegations/index_en.htm);
  by contacting the Europe Direct service (http://europa.eu/europedirect/index_en.htm) or
  calling 00 800 6 7 8 9 10 11 (freephone number from anywhere in the EU) (*).

  (*) The information given is free, as are most calls (though some operators, phone boxes or hotels may charge you).

Priced publications:

- via EU Bookshop (http://bookshop.europa.eu).

LB-NA-28372-EN-N

JRC Mission

As the science and knowledge service of the European Commission, the Joint Research Centre's mission is to support EU policies with independent evidence throughout the whole policy cycle.

EU Science Hub
ec.europa.eu/jrc

@EU_ScienceHub

EU Science Hub - Joint Research Centre

Joint Research Centre

EU Science Hub

Publications Office

doi:10.2788/677808

ISBN 978-92-79-64669-0